Comparison of Convective Heat Transfer Correlations and Their Application to Nuclear Thermal Propulsion Reactors

Dennis Nikitaev, Corey D. Smith, and Kelsa Palomares

Advanced Projects Huntsville, Analytical Mechanics Associates, Huntsville, AL, 35806

Primary Author Contact Information: 702-287-6852, dennis.d.nikitaev@ama-inc.com

DOI: ####

This study analyzes various Nusselt number and friction factor correlations and applies them to a Small Nuclear Rocket Engine model with a Sinusoidal power distribution profile to understand their effects on the temperatures and pressures inside the reactor. A nodal thermal hydraulic solver was used to determine the fluid and channel surface temperatures while also incorporating variable fluid properties and channel roughness. The results showed that the considered friction factors could essentially be used interchangeably given that their difference affected the pressure by less than 1%. However, large variations in the tube surface temperature were obtained for the different Nusselt numbers while the fluid temperature distribution was forced to remain the same. Supersonic flow conditions presented by Maynard Taylor are investigated to serve as a baseline for how experimental errors can lead to uncertainties in the reported empirical correlations. Detailed experimental investigation is necessary to determine the Nusselt number correlation that will provide the best prediction of the thermal hydraulic performance inside the reactor fluid flow channels.

I. INTRODUCTION

The Space Nuclear Propulsion (SNP) project Fuel and Moderator Development Plan (F&MDP) Task 1.10.12 is aimed at determining an average convective heat transfer coefficient inside a fuel element channel of a nuclear thermal propulsion (NTP) engine. The fluid of interest is hydrogen as it has the potential to enable high specific impulse (~900 s, twice the efficiency of the best performing chemical engines) if it is heated to temperatures of ~2700 K or greater. To do this, hydrogen, originally stored in a propellant tank as a liquid, is pumped through engine cooling channels reaching a temperature close to 300 K and pressure in excess of 8 MPa[1]. At these conditions, hydrogen is a supercritical fluid at the reactor entrance. Afterwards, it travels through the reactor which acts as a heat exchanger to transfer the energy from fission to heat the hydrogen propellant. This process typically requires the hydrogen to flow through a fuel channel with a diameter of only a few millimeters and a length of approximately 1 meter under extreme heat fluxes to increase its temperature by around 2400 K. Because of the unique considerations to properly represent the underlying physics and their impact to heat transfer in an NTP reactor, the designer of the fuel elements must be well informed when selecting correlations to model the heat transfer. An accurate heat transfer model allows for reduced uncertainty in the predicted exit temperature of the reactor (governs specific impulse) and maximum fuel temperature (governs available margin prior to fuel melting). For this effort, the primary parameter of interest is the convective heat transfer coefficient, $\hbar$. This parameter is used in Newton's Law of Cooling shown in Eq. (1). Here, $\dot{Q}$ is the rate of heat transfer, A_s is the surface area through which heat transfer occurs, T_w is the surface or wall temperature, and T_b is the bulk fluid temperature. In Eq. (1), $\hbar$ scales $\dot{Q}$ which prompts the importance of accurately determining a way to predict this parameter.

$$\dot{Q} = \hbar A_s (T_w - T_b) \tag{1}$$

To accurately predict $\hbar$, a valid correlation for Nusselt number, Nu, must be selected and calculated for the expected fluid properties of the channel. Nu is a dimensionless parameter that characterizes the ratio of convective heat transfer to conductive heat transfer through the fluid with a simplified expression shown in Eq. (2).

$$Nu = \frac{Convective\ heat\ transfer}{Conductive\ heat\ transfer} = \frac{\hbar}{k/L} = \frac{\hbar L}{k} \tag{2}$$

Here, L is the characteristic length and k is the fluid thermal conductivity. There are many correlations that can be used for predicting Nu across a wide range of applications. For modeling convective heat transfer in the current SNP Testing Reference Design (TRD) reactor, it is important that the selection of Nu is valid for a hydrogen propellant subjected to internal turbulent flow in a small cylindrical channel under high heat flux (i.e. high T_w/T_b), and representative surface roughness (ε). Table 1 summarizes some applicable correlations of Nu and friction factor, f, that could be considered for the SNP TRD. In this study, predicted heat transfer and pressure drop were compared for different applicable Nu and f correlations to current correlations used in analyzing heat

transfer within the SNP TRD. These correlations and their applicability towards NTP are overviewed.

II. BACKGROUND

II.A. Legacy Nusselt and Friction Factor Correlations

A commonly suggested correlation for estimating Nu is the Dittus – Boelter correlation shown in Eq. (3) which is valid for Reynolds numbers (Re) above 10,000 and Prandtl numbers (Pr) between 0.7 and 120 (Ref. 2). However, this correlation does not account for differences between the local wall and bulk temperatures of the fluid and may be inaccurate when the differences are significant ($T_w/T_b \gg 1$). McCarthy & Wolf developed a correlation for fully thermally developed flow which captured these large differences between the bulk and wall surface temperatures ($1.6 < T_w/T_b < 11.1$) specifically for hydrogen and helium and is shown in Eq. (4) (Ref. 3). This correlation is valid for Re between 4,000 and 1.5×10^6. Westinghouse modified this correlation to capture entrance effects and is shown in Eq. (5) (Ref. 4) which is also valid for Re between 4,000 and 1.5×10^6. Here, d is the internal tube diameter and dx is the local length of tube where the correlation is applied. This Westinghouse correlation is the standard correlation used in SNP for reactor-engine power balance modeling.

$$Nu_{DB} = 0.023 Re^{0.8} Pr^{0.4} \tag{3}$$

$$Nu_{M\&W} = 0.025 Re^{0.8} Pr^{0.4} \left(\frac{T_w}{T_b}\right)^{-0.55} \tag{4}$$

$$Nu_W = 0.025 Re^{0.8} Pr^{0.4} \left[1 + 0.3\left(\frac{d}{dx}\right)^{0.7}\right] \left(\frac{T_w}{T_b}\right)^{-0.55} \tag{5}$$

An alternative Nu correlation considered for NTP is the Taylor correlation shown in Eq. (6) which is valid for Re above 2500. This correlation is specifically for hydrogen and helium with large differences between the bulk and wall surface temperatures ($1.5 < T_w/T_b < 8$) and making it viable for NTP applications. Taylor also includes an entrance region contribution to heat transfer which is captured as an exponential relationship with the ratio of bulk fluid and wall surface temperature.

$$Nu_T = 0.021 Re^{0.8} Pr^{0.4} \left(\frac{T_w}{T_b}\right)^{-\left(0.29 + 0.0019\frac{dx}{D}\right)} \tag{6}$$

These Nu correlations do not account for frictional (f) or roughness contributions to convective heat transfer, thus are most accurate and valid for channels which can be characterized as hydraulically smooth[5]. Heat transfer is known to be enhanced by surface roughness (ε). In channels which are far from hydraulically smooth, such as that as an unpolished, as machined surface or a channel formed by many discrete stacked elements, heat transfer and pressure loss can be better described by a Nu correlation and conservation of energy solution which incorporates f and frictional pressure drop contributions respectively. Some applicable correlations for f and Nu correlations which incorporate f are discussed.

Churchill's friction factor is commonly used in NTP modeling for predicting pressure losses. The advantage of using the Churchill friction factor is that it can be used to represent flows within laminar, transitional, and turbulent regions without any restrictions on Re. This correlation is shown in Eq. (7) with constants *A* and *B* defined in Eq. (8) and Eq. (9), respectively[6]. A minor drawback of this equation is that it could be lengthy to incorporate into a code.

$$f_{CH} = 8\left[\left(\frac{8}{Re}\right)^{12} + \frac{1}{(A+B)^{1.5}}\right]^{1/12} \tag{7}$$

$$A = \left[2.457 \ln\left(\frac{1}{\left(\frac{7}{Re}\right)^{0.9} + 0.27\frac{\varepsilon}{d}}\right)\right]^{16} \tag{8}$$

$$B = \left(\frac{37530}{Re}\right)^{16} \tag{9}$$

A Nusselt number correlation that incorporates f contributions to heat transfer is the Nunner correlation shown in Eq. (10) which is valid for Re above 10,000 and Pr above 0.7. This correlation could be a candidate for NTP because it incorporates roughness, is valid in the post-transitional region for fully turbulent flow, and accommodates for large temperature differences between the fluid and the wall surface. Here, f_{smooth} is the chosen friction factor correlation (such as Churchill) evaluated at a channel roughness of 0. The original Nunner correlation used the Fanning friction factor which was changed to use the standard friction factor (without having to divide by 4) (Refs. 7,8).

$$Nu_{Nunner} = \frac{RePr\left(\frac{f}{8}\right)\left(\frac{T_w}{T_b}\right)^{-0.4}}{1 + \frac{1.5}{Re^{1/8}Pr^{1/6}}\left[Pr\left(\frac{f}{f_{smooth}}\right) - 1\right]} \tag{10}$$

Another correlation for Nu which also accounts for surface roughness is Gnielinski shown in Eq. (11) and is valid for Re between 3,000 and 1.5×10^6 and Pr between 0.5 and 2,000. This correlation incorporates the friction factor for a hydraulically smooth flow channel. Since the Woods correlation, seen in Eq. (12), necessitates a rough tube section, this correlation is applicable to all the empirical Nu correlations besides Gnielinski and Nunner. This friction factor has the benefit of being explicitly defined and relatively quick to solve and is valid for Re between 4,000 and 5×10^7 and roughness to hydraulic diameter ratio $\frac{\varepsilon}{D_{hyd}}$ between 1×10^{-5} and 0.04. (Ref. 9)

The Gnielinski correlation accounts for the differences in the Prandtl numbers of the bulk fluid and the fluid at the wall. Furthermore, entrance effects are also considered. This could be a viable correlation for NTP; however, since this correlation is widely used for many different kinds of fluids, it is not specifically catered for NTP operating conditions with a hydrogen working fluid[10].

$$Nu_G = \frac{\frac{f_{smooth}}{8} Pr_b (Re - 1000)}{1 + 12.7\left(\frac{f_{smooth}}{8}\right)^{1/2}\left(Pr_b^{2/3} - 1\right)}\left[1 + \left(\frac{d}{dx}\right)^{2/3}\right]\left(\frac{Pr_b}{Pr_w}\right)^{0.11} \quad (11)$$

$$f_W = 0.094\left(\frac{\varepsilon}{D_{hyd}}\right)^{0.225} + 0.53\frac{\varepsilon}{D_{hyd}} + \frac{88\left(\frac{\varepsilon}{D_{hyd}}\right)^{0.44}}{Re^{1.62\left(\frac{\varepsilon}{D_{hyd}}\right)^{0.134}}} \quad (12)$$

Another viable candidate for f in NTP applications is the Haaland correlation shown in Eq. (13) and does not have any specified limits on the operability regime[8,11]. This friction factor is in good agreement with that predicted by the Moody Chart and is also explicitly defined. A draw back of the Haaland correlation is that it is not applicable to the entire fluid flow regime range from laminar to transitional to turbulent like Churchill. However, for the applications of NTP, the Haaland correlation would suffice. A correction factor of 4 is placed on this correlation since it is calculating the Fanning friction factor.

$$f_H = 4 * \left\{3.4735 - 1.5635 \ln\left[\left(\frac{2\varepsilon}{D}\right)^{1.11} + \frac{63.6350}{Re}\right]\right\}^{-2} \quad (13)$$

The last friction factor correlation considered is the Darcy – Weisbach correlation shown in Eq. (14) and is valid for Re greater than 10,000. This correlation is transcendental and requires numerical methods for determining the friction factor. It is a good choice for NTP because it is the basis for the Moody Chart – the standard in predicting the friction factor based on *Re*, duct diameter, and roughness.

$$\frac{1}{\sqrt{f_{DW}}} = -2\log_{10}\left(\frac{\varepsilon/D}{3.7} + \frac{2.51}{Re\sqrt{f_{DW}}}\right) \quad (14)$$

II.B. Taylor Experiments Mach Number Limitations

Pertinent heat transfer and fluid mechanical phenomena at elevated temperatures, such as the heat transfer coefficient and friction factor, rely on historical empirical correlations to properly model the thermal hydraulics of the reactor flow channels and engine subcomponents. As discussed in Section II.A., these correlations typically involve limited operability regimes and are based on an extended list of non-trivial assumptions. Experiments performed by Maynard Taylor[12,13] provide seemingly useful empirical correlations for the heat transfer coefficient that have been leveraged in numerous modeling activities by NASA and industry. Deeper investigation into the reported temperature and pressure data introduces flow regime concerns at the exit of the test rig. The Mach number (M) of the fluid enters the test article in a subsonic state before reaching choked flow (M > 1) at the exit plenum for nearly every test case.

Temperature measurements reported by Taylor can be assumed as stagnation values since the instrumentation is located in the plena of the test rig. Pressure measurements represent static values for both the entrance and exit of the test section. To determine the M regime of the fluid, isentropic and isobaric, or constant entropy and pressure, conversions between stagnation and static temperatures are performed based on Eq. (15) (Ref. 14):

$$T_{stag} = T_{stat} * (1 + 0.5 * M * (\gamma(P, T_{stat}) - 1)) \quad (15)$$

Since Eq. (15) includes the calculated M, an iterative loop to converge on the static temperature and M simultaneously is a simple way to solve the complex equation form. In Eq. (15), γ is defined as the ratio between the specific heat at constant pressure and specific heat at constant volume of the working fluid at the static temperature. These properties are dependent on the entrance and exit state points, so updates to these values should be performed each iteration. Fluid properties such as density and γ can be identified at a constant static pressure and the calculated static temperature from Eq. (15). Base fluid mechanical equations for solving the fluid velocity (Eq. (16)) and Mach number (Eq. (17)) are dependent on these hydrogen properties.

$$v_{fluid} = \frac{\dot{m}}{A_{flow} * \rho(P, T_{stat})} \quad (16)$$

$$M = \frac{v_{fluid}}{\sqrt{\frac{\gamma(P, T_{stat}) * P}{\rho(P, T_{stat})}}} \quad (17)$$

Outputs from Eq. (16) and Eq. (17) below are compared with prior iteration values by a percent error calculation until a high-fidelity convergence criterion is met. Results from this methodology for various Taylor test cases are found in Section IV.C. State point-specific Mach numbers are calculated through isentropic physical relations between the tabulated stagnation temperatures and associated static temperatures at a constant static pressure. Through this back calculation at the entrance and exit of the test section, a transition from the subsonic to supersonic flow regime exists in nearly every reported test case. The reported data from the Taylor experiments can be deemed inappropriate due to this flow regime transition and the associated changes to the physical modeling of the system. Future experimental test cases should limit the Mach number regime to prototypic conditions seen in nuclear thermal rocket designs to increase the applicability of the derived empirical model.

III. METHODOLOGY

III.A. Nodal Thermal Hydraulic Solver

To identify heat transfer and pressure loss trends across a prototypic NTP fuel channel, a reference design is required. The Small Nuclear Rocket Engine (SNRE) model is chosen to be the representative test case since it covers the temperature/pressure regimes expected in operational reactor concepts and is not export-controlled. Engine-reactor state points, fuel element geometry, and power levels are extracted from the reference design and converted into a 1-D axial flow channel model[12]. Table 2 lists the system conditions incorporated in this thermal hydraulic solver.

Table 2: SNRE System Conditions and State Points[13]

Parameter	Value/Units
Total Mass Flow Rate	8.31 kg/s
Reactor Inlet Temperature	372.1 K
Reactor Inlet Pressure	3.96 MPa
Reactor Length	890 mm
Channel Pitch	4.1 mm
Flow Channel Diameter	1.3 mm
Clad Thickness	0.1 mm
Total Reactor Power	367 MWt
Average Power Density	3.394 MWt/L

The 1-D axial flow channel solver relies on a control volume mesh approach with node-specific power deposition, pressure, and temperature. An iterative sequence is utilized to calculate the system parameters at each node based on the data from the previous node, commonly referred as a "forward-difference" methodology. Since some of the proposed empirical correlations rely on the wall and fluid bulk temperature, an additional iterative convergence is performed on each node to accurately measure the wall temperature based on the fluid properties and power level. Following successful convergence of the fluid and wall temperature distributions, the Sparrow equation is used to calculate the maximum and average fuel temperature based on a hexagonal unit cell surrounding the channel with reflective boundary conditions[13]. Similar to the thermal hydraulic solver, the Sparrow equation incorporates the node-specific power deposition to calculate the temperature gradient across the fuel meat.

III.B. Heat Deposition Function

The heat deposition function provided a heat profile along the axial length *L* of the test article. This is done by translating the total power $\dot{Q}_{tot}$ and an optional curve parameter into an analytical mathematical function which provides the heat deposited per unit length at the specified location $\dot{Q}(x)$. The currently available options for curve shapes include Flat, Sinusoidal, Linear, and Exponential. The Flat curve is the simplest and consists of simply taking the total power and dividing it by the total axial length yielding a constant heat deposition value throughout the entire axial length of the test article. The Sinusoidal option uses the heat deposition Sine function shown in Eq. (18). By integrating this function, the code automatically determines the amplitude *A* of the curve given $\dot{Q}_{tot}$ and *L* as shown in Eq. (19).

$$\dot{Q}(x) = A \sin\left(\frac{\pi}{L}x\right) \tag{18}$$

$$\dot{Q}_{tot} = \int_0^L A \sin\left(\frac{\pi}{L}x\right) dx = \frac{2AL}{\pi} \rightarrow A = \frac{\dot{Q}_{tot}\pi}{2L} \tag{19}$$

The Linear option also takes the $\dot{Q}_{tot}$ and *L* inputs as well as the desired slope in watts/meter as an additional input. This function is based on the line equation $\dot{Q}(x) = mx + b$ where the slope m is user defined and b is found by integrating the line equation and setting it equal to $\dot{Q}_{tot}$ as shown in Eq. (20).

$$\dot{Q}_{tot} = \int_0^L (mx + b)\, dx = \frac{mL^2}{2} + bL \rightarrow b = \frac{\dot{Q}_{tot} - mL^2}{L} \tag{20}$$

Similarly, the Exponential option also takes an additional input that serves as the modifier λ of the exponential function $\dot{Q}(x) = A\exp(\lambda x)$. Here, scaling parameter *A* is determined from integrating the exponential function and setting it equal to $\dot{Q}_{tot}$ as shown in Eq. (21).

$$\dot{Q}_{tot} = \int_0^L A\exp(\lambda x)\, dx = \frac{A}{\lambda}[\exp(\lambda L) - 1] \rightarrow A = \frac{\dot{Q}_{tot}\lambda}{\exp(\lambda L) - 1} \tag{21}$$

By incorporating these analytical heat deposition functions into the Nodal Thermal Hydraulic Solver, the fluid temperature is determined along the length of the test tube.

IV. RESULTS

The baseline case that uses the Westinghouse Nusselt number and Churchill friction factor correlation is shown in Fig. 1. As was discussed previously, the Westinghouse Nusselt number correlation incorporates the length of the tube and the steep wall temperature results at the tube entrance. Then the wall temperature relatively evens out and converges with the fluid temperature at the tube exit. The shape of this curve between 0.2 m and 0.9 m is primarily due to the power curve produced by Eq. (18). The pressure gradient $\frac{dP}{dx}$ decreases along the tube due to decreasing density as the temperature increases while the internal flow diameter of the tube stays the same.

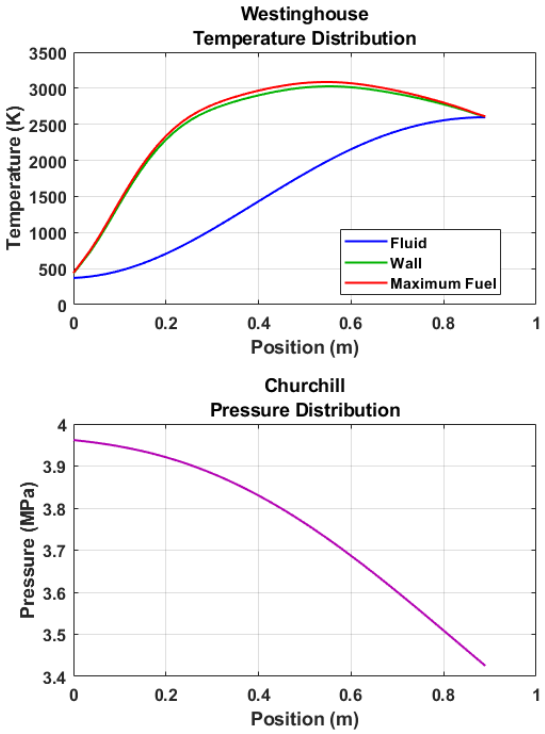

Fig. 1: Baseline Case

IV.A. Friction Factors

The friction factors are compared against the Space Nuclear Propulsion (SNP) baseline: Westinghouse Nusselt number correlation using the Churchill friction factor correlation. The tube diameter is set to be 2.3 mm and a tube length of 0.9 m. Fig. 2 shows the variation of the friction factors which follow the same trend. Fig. 3 shows that the differences between these friction factor correlations and the Churchill correlation are less than 4%. According to numerical model comparison guidelines, these differences are within an acceptable tolerance of 4% (Ref. 14).

In the case of the baseline, the friction factor affects the pressure losses and not the Nusselt number as the Westinghouse correlation is independent of the friction factor as indicated by Eq. (5). The effect on the pressure losses is shown in Fig. 4 where the apparent difference caused by the different friction factors is small. Furthermore, the difference in the fluid pressures at any given position along the tube is less than 1% as shown in Fig. 5 which is well within the acceptable tolerance of 4% for numerical modeling[14].

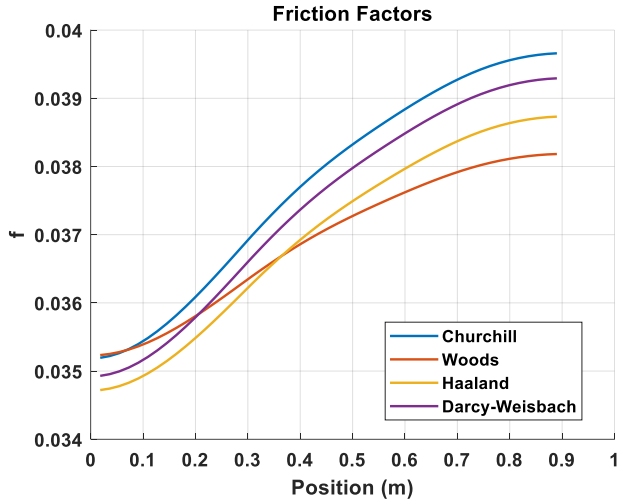

Fig. 2: Friction Factors

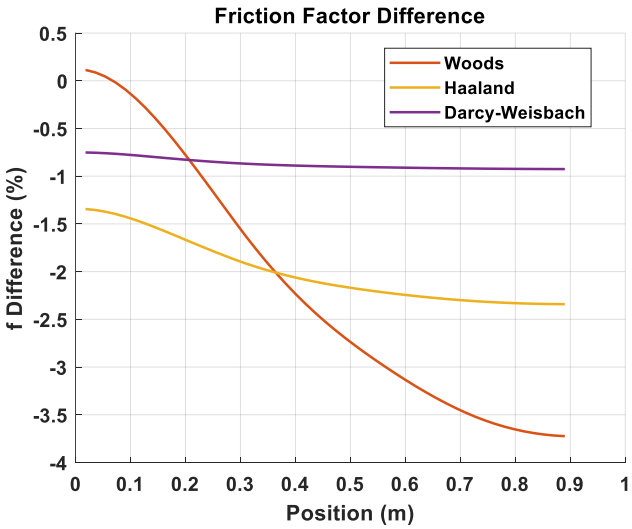

Fig. 3: Friction Factor Difference

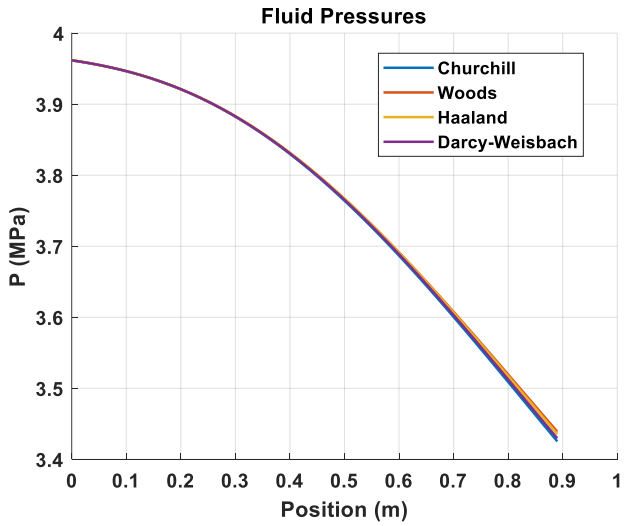

Fig. 4: Fluid Pressures

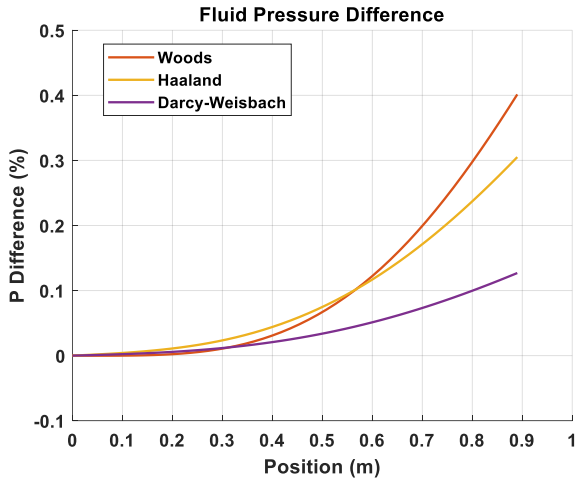

Fig. 5: Fluid Pressure Difference

IV.B. Nusselt Numbers

The comparisons among the Nusselt number correlations will use the SNP baseline Westinghouse Nusselt number with the Churchill friction factor correlations for consistency and uniformity. However, as was shown, the differences between these comparisons will not depend significantly on the friction factor correlation used. The Nusselt number correlations are dependent on the Reynolds and Prandtl numbers which also depend on the fluid properties. To provide a uniform comparison, the Reynolds, Prandtl, fluid temperature, and fluid pressure parameters were kept the same which will cause variations to the required wall temperature based on the Nusselt number correlation.

The comparison of the Nusselt number correlations is shown in Fig. 6 and the percent differences are shown in Fig. 7 which are compared to the Westinghouse correlation. The thermal entrance effects are categorized by a large negative initial slope of the Nusselt number that transitions into a steady trend. Both the Westinghouse and McCarthy & Wolf correlations, that were specifically developed for hydrogen and helium flow, have the lowest thermal entrance length of about 100 tube diameters. The Taylor correlation exhibits a thermal entrance length of about 150 tube diameters but then begins increasing. The increasing trend is due to the resulting high temperature differences between the bulk fluid and surface given the low Nusselt number. If closely observed, both the Westinghouse and McCarthy & Wolf correlations show slight increasing in the Nusselt numbers which can also be attributed to the surface and bulk fluid temperature differences. The Nunner correlation has the longest thermal entrance length of about 175 tube diameters of all correlations that account for the thermal entrance effects. These thermal entrance effects indicate that the classical academic rule of thumb that the thermal entrance length is 10 tube diameters long is off by an order of magnitude from what these correlations indicate.

The Westinghouse, McCarthy & Wolf, and Taylor correlations assume smooth tubes and do not incorporate a friction factor which promotes the mixing of the boundary layer fluid with the core fluid. The Nunner correlation, on the other hand, incorporates the surface roughness in the form of a friction factor which results in a relatively constant Nusselt number toward the end of the channel which is what would be expected once the flow becomes thermally fully developed. The Gnielinski and Dittus-Boelter correlations exhibit the largest errors likely due to their generalized applicability to various flow applications and fluids. These correlations predict the largest Nusselt number and do not achieve fully thermally developed flow since a constant value is never approached.

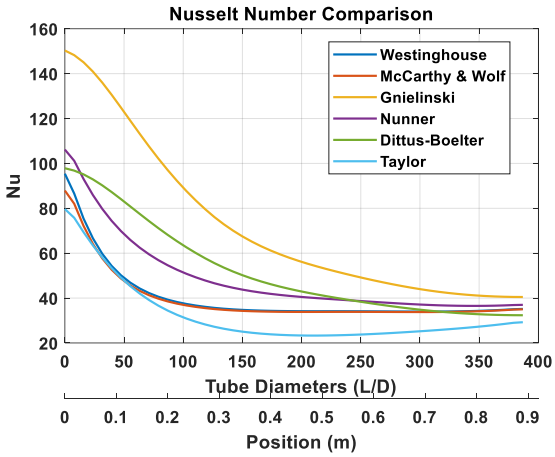

Fig. 6: Nusselt Numbers

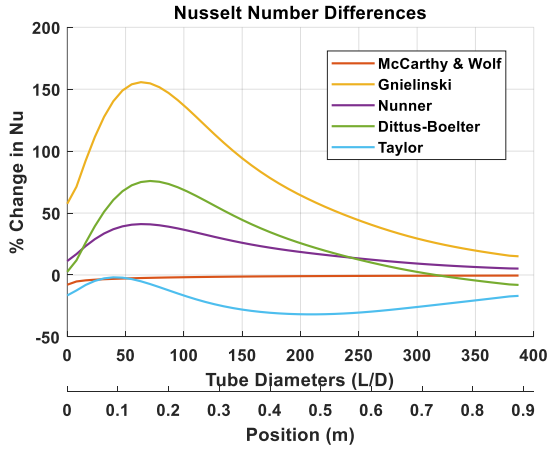

Fig. 7: Nusselt Number Difference

As previously discussed, the Nusselt number correlations primarily impact the wall temperature. Fig. 8 shows the bulk fluid temperature (black dashed curve) and how the wall temperatures which result from the different correlations compare to the fluid temperature. Both the Westinghouse and McCarthy & Wolf correlations are very close together which is consistent with the fact that the only difference between these correlations is Westinghouse's

consideration of the entrance region. Since the Taylor correlation resulted in the smallest Nusselt number, the resulting wall temperature is the highest of all correlations. Similar results are seen in the Nunner, Dittus-Boelter, and Gnielinski correlations that are consistent with the Nusselt number values shown in Fig. 6. The wall temperature percent differences are shown in Fig. 9 which have the same shapes as the Nusselt number differences of Fig. 7 except that they are flipped along the x-axis indicating the inverse relationship between the Nusselt number and the wall temperature.

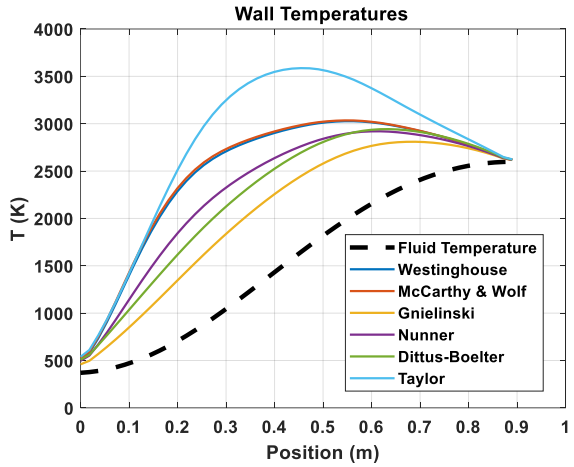

Fig. 8: Wall Temperatures

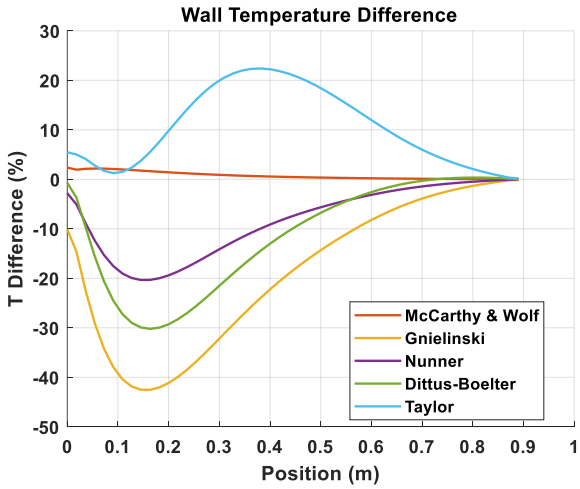

Fig. 9: Wall Temperature Difference

IV.C. Taylor Choked Flow Test Cases

Testing the flow conditions and state points reported by Taylor determines the applicability of these heat transfer and friction factor correlations to future SNP work tasks. The axial wall temperature distribution for each case undergoes a large temperature change in a short distance near the channel exit due to temperature feedback from a water-cooled electrical channel found in both plena of the testing apparatus which altered the outlet fluid temperature. Knowledge of this phenomena adds uncertainty to the data set and associated empirically derived correlations. Taylor did not include specific values outside of the plotted wall temperature data, so a back calculation to find the exact choke point location along the tube length is not trivial.

The simulated results of the iterative methodology, as presented in Tables 3 and 4, provide key insight into the supersonic flow regime found in almost all of Taylor's experiments. Fluid velocity, static temperature, stagnation temperature, and the case-specific Mach number at the tube entrance and exit are found in the tables below.

Table 3: Sample Case Output Conditions at Inlet

	Case 1	Case 20	Case 46	Case 49
Velocity [m/s]	396.37	242.61	210.64	136.41
Static T [K]	310.24	310.23	144.72	163.87
Stag. T [K]	315.56	312.22	146.11	164.44
Mach Number	0.2973	0.1820	0.2348	0.1431

The Mach number range seen at the inlet allows the fluid flow to remain in the incompressible regime. This observation is beneficial for structural stability of the test rig since acoustic oscillations and other vibrational effects will not be observed at the entrance. Case 1 approaches the 0.3*M boundary between incompressible and transonic flow, but the value is not the extremes seen at the exit in Table 4. Typically, SNP reactor coolant channels are designed to stay within this incompressible flow regime with significant margin to avoid vibrational events during in-flight reactor operation. Another interesting takeaway from Table 3 includes the small difference between static and stagnation temperatures. This small change can be attributed to the low Mach number and the small deviation in the specific heat ratio, γ, at low temperatures.

Table 4: Sample Case Output Conditions at Outlet

	Case 1	Case 20	Case 46	Case 49
Velocity [m/s]	1838.70	2857.21	1367.80	2659.63
Static T [K]	514.22	1055.20	414.55	1071.81
Stag. T [K]	630.56	1325.56	478.89	1305.56
Mach Number	1.0683	1.1675	0.8853	1.0787

While Case 46 in Table 4 does not reach a Mach number above unity, the value is close enough to be considered transonic flow. Transonic flow in a tube correlates to a fluid speed that approaches the medium-specific speed of sound, leading to possible localized supersonic flow at the higher temperature convection boundary layer. Transonic flow regimes found using averaged fluid properties is undesirable for SNP applications, so this run case is problematic as well. Lower heat rate and higher mass flow rate cases, such as Cases 1 and 46, result in a smaller temperature and Mach number gradient between the entrance and exit. However, these runs see a higher inlet Mach number due to the elevated mass flow rate and wall temperature. In contrast to the Table 3 results, the stagnation and static temperature

difference is significantly greater for the exit plenum due to the increased magnitude of the Mach number. The higher coolant velocity and lower pressure value at the exit are the key drivers of the elevated mass flow rate based on Eq. (16) and Eq. (17).

Presence of a choke point downstream in a constant flow area test section with an entrance subsonic flow regime without rapid pressure variations typically violates the Second Law of Thermodynamics. Minimal accepted literature discusses this phenomena due to the limited use case in physical applications, yet this flow behavior occurs in essentially all of Taylor's reported test cases. Shapiro[14] introduces the possibility of subsonic to supersonic flow transition after a choke point due to extreme changes in heat input or losses to the flow along the test section. Taylor plots the axial distribution of the wall temperature which shows a rapid temperature differential at the end of the test section due to external tube cooling mechanisms. Due to this rapid heat loss, instabilities in the flow regime enables the flow to transition from initially subsonic to the supersonic range. The results in Tables 3 and 4 provide clarity on this transition by presenting Mach number deviations at the entrance and exit of the test section.

V. CONCLUSION

Based on these results, the effects of the thermal entrance region may be a great area of concern for the average heat transfer coefficient experiment. The academic rule of thumb on the thermal entrance length of being 10 tube diameters does not seem to apply to this application and is an order of magnitude below the predicted values. The Dittus-Boelter and Nunner correlations are not applicable to this analysis as the Prandtl number is below 0.7. It is possible that the length of the test article will need to be longer or the diameter of the channel smaller to mitigate, at least partially, the thermal entrance effects. The Gnielinski correlation predicted the highest Nusselt number of all considered correlations likely due to its wide applicability to general heat transfer applications and not necessarily catered to the conditions found inside the NTP reactor. The Dittus-Boelter correlation does not account for the thermal entrance effects. This results in a different predicted Nusselt number trend where the Nusselt number slope at the channel entrance is close to zero. The predicted trend then begins to exhibit the thermal entrance effects for a much longer length than the correlations which incorporate these effects. Therefore, it is of interest to use correlations which are specifically designed to predict these thermal entrance effects.

ACKNOWLEDGMENTS

This work was supported by NASA's Space Technology Mission Directorate (STMD) through the Space Nuclear Propulsion (SNP) project. This work was funded under Contract No. 80LARC17C0003. The SNP Modeling and Simulation (M&S) Lead, Jonathan McDonald, provided background information and technical review for this effort.

REFERENCES

[1] Joyner, C. R., Eades, M., Horton, J., Jennings, T., Kokan, T., Levack, D. J. H., Muzek, B. J., and Reynolds, C. B. "LEU NTP Engine System Trades and Mission Options." *Nuclear Technology*, Vol. 206, No. 8, 2020, pp. 1140–1154. https://doi.org/10.1080/00295450.2019.1706982.

[2] Çengel, Y. A., and Ghajar, A. J. *Heat and Mass Transfer: Fundamentals & Applications*. McGraw-Hill, New York, 2011.

[3] McCarthy, J., and Wolf, H. *THE HEAT TRANSFER CHARACTERISTICS OF GASEOUS HYDROGEN AND HELIUM*. Publication NP-10572, RR-60-12, 4842792. 1960, p. NP-10572, RR-60-12, 4842792.

[4] Thomas, G. R. *An Interim Study of Single Phase Heat Transfer Correlations Using Hydrogen*. Publication WANL-TNR--056, 4233809. 1962, p. WANL-TNR--056, 4233809.

[5] Jennings, T., Witter, J., Joyner II, C. R., and Hanks, A. *Modeling of Fuel Element Thermal Hydraulic Performance of a Fuel Element and Reactor Integration for a Nuclear Thermal Propulsion System (ITAR)*. Aerojet Rocketdyne.

[6] Churchill, S. W. "Friction-Factor Equation Spans All Fluid-Flow Regimes." *Journal of Chemical Engineering*, Vol. 84, No. 24, 1977, pp. 91–92.

[7] Nunner, W. *Heat Transfer and Pressure Drop in Rough Tubes*. Atomic Energy Research Establishment, 1958.

[8] *Mathcad - Reynolds Range and Candidate Nusselt Correlation with Roughness for New Experiment*. Analytical Mechanical Associates.

[9] Emrich, W. *Principles of Nuclear Rocket Propulsion*. Butterworth-Heinemann, an imprint of Elsevier, Oxford, United Kingdom, 2016.

[10] Men, Q., Wang, X., Zhou, X., and Meng, X. "Heat Transfer Analysis of Passive Residual Heat Removal Heat Exchanger under Natural Convection Condition in Tank." *Science and Technology of Nuclear Installations*, Vol. 2014, 2014, pp. 1–8. https://doi.org/10.1155/2014/279791.

[11] Haaland, S. E. "Simple and Explicit Formulas for the Friction Factor in Turbulent Pipe Flow." *Journal of Fluids Engineering*, Vol. 105, No. 1, 1983, pp. 89–90. https://doi.org/10.1115/1.3240948.

[12] Taylor, M. F. *Experimental Local Heat-Transfer and Average Friction Data for Hydrogen and Helium Flowing in a Tube at Surface*

Temperatures up to 5600^{0}R. Publication NASA TN D-2280. 1964.

[13] Taylor, M. F. *Experimental Local Heat-Transfer Data for Precooled Hydrogen and Helium at Surface Temperatures up to 5300^{0}R*. Publication NASA TN D-2595. National Aeronautics and Space Adminstration, Washington D.C., 1965.

[14] Shapiro, A. H. Section 8.10. In *The Dynamics and Thermodynamics of Compressible Fluid Flow*, The Ronald Press COmpany, New York, 1953, pp. 256–258.

[15] Patel, V., Eades, M., and Joyner II, C. R. *SPOC Benchmark Case: SNRE Model*. Publication INL/CON-15-37189. Idaho National Laboratory, Idaho Falls, ID, 2016.

[16] Sparrow, E. M. "Temperature Distribution and Heat-Transfer Results for an Internally Cooled, Heat-Generating Solid." *Journal of Heat Transfer*, Vol. 82, No. 4, 1960, pp. 389–392. https://doi.org/10.1115/1.3679965.

[17] Mayorca, M. A. *Numerical Methods for Turbomachinery Aeromechanical Predictions*. Dissertation. Royal Institute of Technology, Stockholm, Sweden, 2011.